J. Fluid Mech. (2001), *vol.* 449, *pp.* 169–178.
DOI: 10.1017/S0022112001006310 Printed in the United Kingdom

The wind in confined thermal convection

By J. J. NIEMELA[1], L. SKRBEK,[1,2]
K. R. SREENIVASAN[3] AND R. J. DONNELLY[1]

[1]Cryogenic Helium Turbulence Laboratory, Department of Physics, University of Oregon, OR 97403, USA

[2]Low Temperature Laboratory, Institute of Physics ASCR and Charles University, 180 00 Prague, Czech Republic

[3]Mason Laboratory, Yale University, New Haven, CT 06520, USA

(Received 13 June 2001 and in revised form 30 August 2001)

A large-scale circulation velocity, often called the 'wind', has been observed in turbulent convection in the Rayleigh–Bénard apparatus, which is a closed box with a heated bottom wall. The wind survives even when the dynamical parameter, namely the Rayleigh number, is very large. Over a wide range of time scales greater than its characteristic turnover time, the wind velocity exhibits occasional and irregular reversals without a change in magnitude. We study this feature experimentally in an apparatus of aspect ratio unity, in which the highest attainable Rayleigh number is about 10^{16}. A possible physical explanation is attempted.

1. Introduction

A fascinating but poorly understood feature of fully developed turbulence is the ubiquitous presence of organized motion embedded in a background of strong fluctuations. For the turbulent flow set up by thermal convection in a closed box, several organized features of motion, such as plumes, jets, and the large-scale circulation, are known to exist (e.g. Kadanoff 2001). The wind is the large-scale circulation whose size is of the order of a convection cell (although perhaps distinct from the large-scale flow across several cells discussed by Krishnamurti & Howard 1981). Here, we are primarily concerned with the wind: What are its characteristics, in particular, its long-time dynamics? How does it arise and what causes an occasional and irregular reversal of its direction? We present experimental results on these issues. Although other groups have reported similar reversals in wind direction (e.g. Sano, Wu & Libchaber 1989; Ciliberto, Ciono & Laroche 1996), there has not yet been a systematic investigation of its dynamics.

A measure of the ratio of the effect of buoyancy, which tends to accelerate a fluid parcel upwards, to the viscous and diffusive effects, which tend to slow it down, is the Rayleigh number, $Ra \equiv \alpha \Delta g L^3/\nu\kappa$. Here α is the isobaric thermal expansion coefficient of the fluid in the container, Δ is the temperature difference between the bottom and top walls, g is the acceleration due to gravity, L is the vertical dimension of the convection cell, ν is the kinematic viscosity of the fluid and κ its thermal diffusivity. In many practical circumstances, Ra is very large; in the present experiments, Ra spans the range between 10^6 and 10^{16}, and the wind is defined with reasonable certainty at least up to $Ra = 10^{13}$.

2. The apparatus and the measurement of the wind

The container has a circular cross-section of 50 cm diameter, and a height of 50 cm. Thus, the aspect ratio Γ, defined as the ratio of the horizontal dimension to the vertical dimension of the apparatus, is unity. The working fluid is cryogenic helium gas. By varying the operating pressure and temperature of the gas as well as the overheat, the Rayleigh number can be varied between 10^6 and 10^{16}. One of the attractive features of cryogenic helium gas is that this large range of Ra can be produced in a single apparatus.

The apparatus was identical to that used by Niemela *et al.* (2000), except that the latter was 100 cm high and $\Gamma = 1/2$. The top and bottom plates were made of copper that was annealed under oxygen-free conditions to have, at an illustrative temperature of 5 K, a high thermal conductivity of about 2 kW m^{-1} K^{-1}. Special efforts were made to heat the plate uniformly along its surface. The sidewall was made of thin stainless steel. The apparatus was insulated by three thermal shields and vacuum chambers at various graded temperatures. The top wall was connected to a helium reservoir through a distributed and adjustable thermal link, and its temperature was maintained constant by means of a resistance bridge and servo.

As in Niemela *et al.* (2000), temperature fluctuations were measured by small sensors made of neutron-transmutation-doped germanium crystal cubes, 250 μm on a side. The majority of the data on the large-scale circulation discussed here result from a pair of sensors placed a radial distance $w = 4.4$ cm from the sidewall on the horizontal mid-plane. They were aligned vertically and separated by a distance $d = 1.27$ cm. These sensors were each a part of a separate bridge circuit, with temperature fluctuations $\theta_1(t)$ and $\theta_2(t)$ sampled at a frequency of 50 Hz over long times (see § 3). If the convective motion consisted only of a steady wind with some periodic modulation, the temperature signals from the sensors near the sidewall would be identical, with a well-defined phase lag given by their separation and the magnitude of the wind velocity; a variant of this idea works also in the presence of background turbulence (e.g. Sano *et al.* 1989). Define a short-time correlation between θ_1 and θ_2 as

$$G(\tau) = \sum_{i=1}^{i=N} \theta_1(t_i)\theta_2(t_{i+n}), \tag{2.1}$$

where t_i is the ith sample of a digitized signal, $\tau = t_{i+n} - t_i$, and the window width N used for calculating the correlation is approximately equal to one convective turnover time for the large-scale flow (about 30 s). As discussed below, this is the optimal window size that can be used for determining the wind velocity. The delay time τ_M for which G has a maximum defines the average phase lag between the two signals θ_1 and θ_2. The wind velocity V is then given by $V = d/\tau_M$ (noting that τ_M could be positive or negative). Clearly, the method cannot resolve fluctuations that oscillate more rapidly than N. The value of N is optimized here to best measure the large-scale circulation; although the numbers obtained are not too sensitive to the window width within a certain range, too small a value of N yields a large variability of $G(\tau)$ while too large a value diminishes the maximum of $G(\tau)$.

3. Main results for the wind

Figure 1 shows a segment of the wind velocity data for $Ra \approx 1.5 \times 10^{11}$. It is clear that $V(t)$ reverses direction† irregularly, and does so quite suddenly. By sudden, we

† Because of the cylindrical symmetry, it is equally valid to suppose that the wind rotates azimuthally by 180°, and it is hard to ascertain which description is more apt. So we simply describe

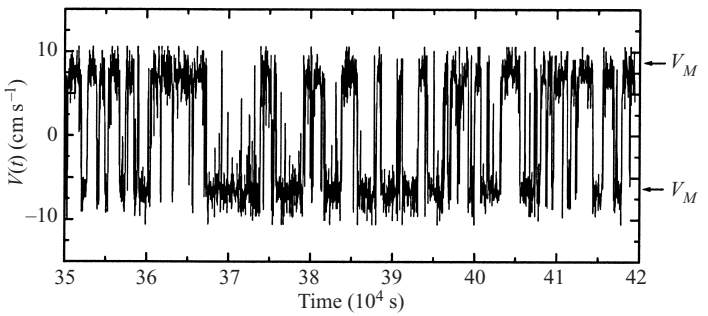

FIGURE 1. The wind velocity as a function of time, obtained as described in the text, for $Ra = 1.5 \times 10^{11}$. The velocity is seen to switch direction swiftly with no apparent order. The arrows on the right indicate its magnitude when it persists in either direction. One of the limitations of the method of measurement using equation (2.1) is that it occasionally yields spuriously large magnitudes. A seemingly benign data-processing criterion, such as neglecting velocities greater than, say, $2V_M$, eliminates all spurious and unphysical spikes.

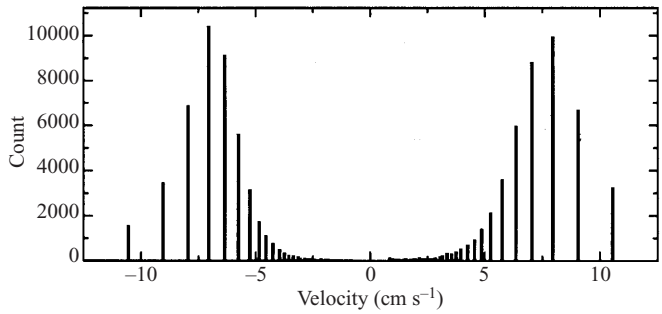

FIGURE 2. Histogram of the wind velocity $V(t)$ for $Ra = 1.5 \times 10^{11}$. The lines are discrete because in the definition $V = d/\tau_M$, d is fixed but τ_M is measured in discrete units of sampling time intervals. The lines become more sparse for larger V because the corresponding values of τ_M are smaller.

mean that the reversal occurs in a time span less than a turnover time. To properly account for dynamical processes occurring at the lowest frequencies in the range the wind velocity was recorded continuously over a duration of about $5\frac{1}{2}$ days. These measurements were begun after the apparatus had been kept at constant experimental conditions for nearly one month, resulting in a very stable initial state. The arrows to the right of figure 1 give a reasonably unambiguous estimate for the magnitude of the mean wind speed, V_M, which is the same to a good approximation for the two orientations of the flow.

That the wind is one large cell on the order of the size of the container rather than, say, two cells of half the size, is easily verified experimentally by noting that: (i) the sensors mounted at 180° about the azimuth indicate the opposite sense of flow and reversals, and (ii) temperature fluctuations near the centre of the cell do not show any evidence of the wind.

The histogram of the wind velocity, shown in figure 2, is bimodal. While the width of each mode, which represents the variability in V_M, depends on various details of

the phenomenon as wind velocity reversal. Cylindrical symmetry can be expected to lead to a slowly precessing wind, but this state is non-generic. That the wind is pinned down between reversals indicates the presence of some benign symmetry breaking in the box (e.g., welding seams).

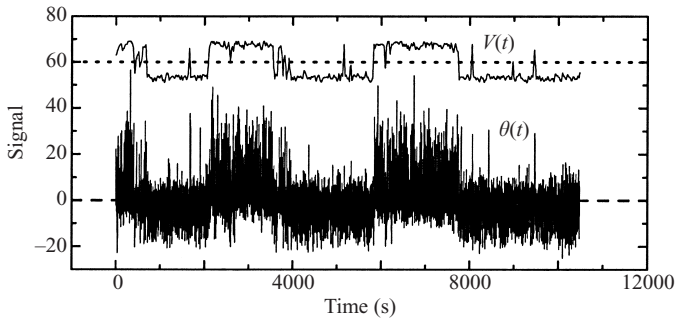

FIGURE 3. The upper trace is a segment of the wind velocity, $V(t)$, somewhat smoothed in comparison to figure 1. The lower trace is the temperature fluctuation, $\theta(t)$, from one of the two sidewall sensors used to determine it (the other is closely similar). The correlation between the wind direction and the large-scale temperature fluctuation is obvious. The velocity trace is symmetric about zero but shifted upwards to $60\,\mathrm{cm\,s^{-1}}$ to avoid overlap. The positive and negative excursions of the temperature fluctuations correspond to relatively warmer and colder fluid respectively, and match the reversal of $V(t)$. $Ra = 1.5 \times 10^{11}$.

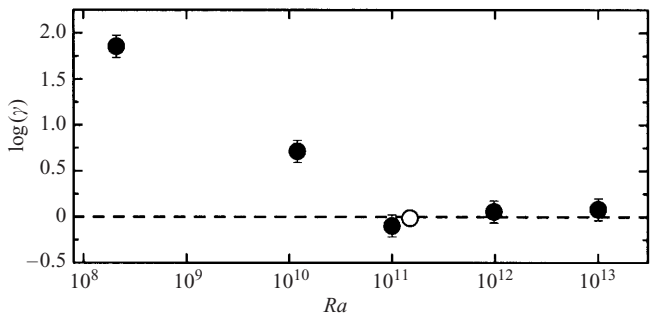

FIGURE 4. The magnitude of the logarithm of the ratio γ (see text) as a function of Ra. For $Ra > 10^{11}$, the wind seems to be on average as often in one direction as the other. The closed symbols represent the average for 3 hours of data, the open symbol for 131 hours.

the measurement and is therefore not easy to interpret precisely, the relative size of the two modes is clearly the long-term tendency for the wind to occur in one direction over the other. For this value of Ra, the wind was observed to change direction as often in one direction as in the other; the amount of time spent in either direction was the same to within 1.4%.

Figure 3 shows the simultaneously obtained traces of the wind and the temperature. There is an unmistakable connection between the hotter fluid and the upward moving wind, and vice versa. The positive and negative parts of the temperature, corresponding to relatively warmer and colder fluid respectively, match the sign reversal in $V(t)$. This may be thought to confirm the validity of the procedure used for measuring the wind.

As Ra is varied, the fraction of time that the wind is in one or the other direction also varies. It favours one of the directions at lower Ra; we do not understand clearly how this direction is determined, but guess that a variety of small variables and initial conditions play a role. If we measure the parameter γ, defined as the ratio of the total time that the wind is in one direction to that in the opposite direction, this parameter varies with Ra as shown in figure 4. The lower the Ra, the more persistently the wind maintains its direction, and the two modes of the histograms of the wind become

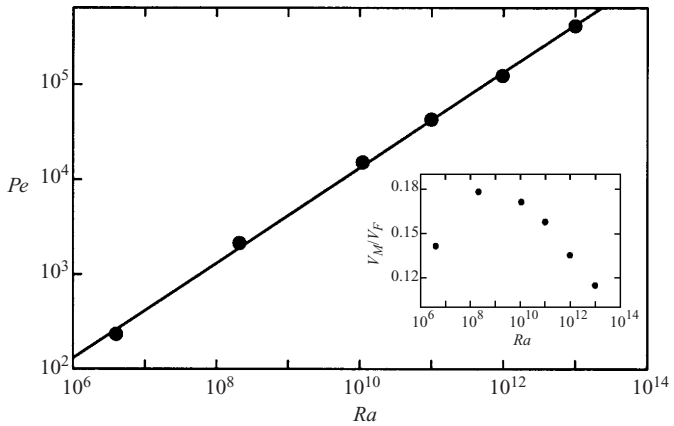

FIGURE 5. The variation of the Péclet number Pe based on the mean wind with Ra over the range where a judicious implementation of the measurement technique is possible. The line corresponds to $Pe = 0.13Ra^{0.50}$. The inset shows V_M as a fraction of the free-fall velocity V_F for various Ra (see text).

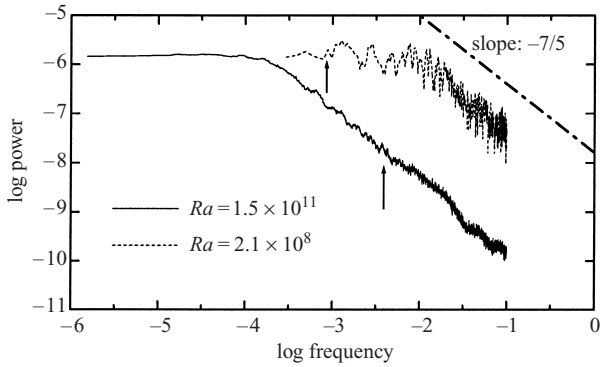

FIGURE 6. Power spectral density for $Ra = 1.5 \times 10^{11}$ and 2.1×10^8. The data for $Ra = 1.5 \times 10^{11}$ were obtained over a very long time span (see text). The dot-dashed line has a slope of $-7/5$. For reference, the arrows indicate the mean crossing frequency of $V(t)$.

increasingly unequal. For $Ra > 10^{11}$, the wind essentially maintains its statistical symmetry (i.e. it is on average as often in one direction as the other). These features were also found for aspect ratio 1/2 (Niemela *et al.* 2000).

At least up to the Ra for which V_M can be measured without much ambiguity, one can define a Péclet number $Pe \equiv Re\,Pr = |V_M|L/\kappa$. It follows the relation (figure 5)

$$Pe = 0.13Ra^{0.50}, \tag{3.1}$$

in general agreement with previously known results, for example, from Sano *et al.* (1989) and Castaing *et al.* (1989); see also Kerr (1996) and Ashkenazi & Steinberg (1999). For stricter comparison to these authors we note that adopting different exponents for the Pr-dependence results in small changes in the Ra-dependence; for example, $RePr^{0.72} \propto Ra^{0.49}$ and $RePr^0 \propto Ra^{0.47}$. In the inset to figure 5 we plot the speed V_M as a fraction of the so-called free-fall velocity, given by $V_F = (\alpha \Delta g L)^{1/2}$. This ratio varies between 0.12 and 0.18 over the range of Ra covered here.

In figure 6 we plot the power spectral densities of the wind velocity V_M for $Ra = 2.1 \times 10^8$ and 1.5×10^{11}. The power-law roll-off at high frequencies is the same

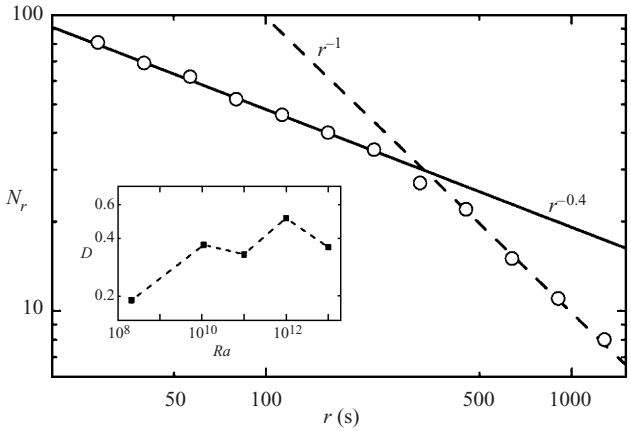

FIGURE 7. A log-log plot of N_r vs. r for $Ra = 1.1 \times 10^{10}$. The existence of a power-law behaviour for small r suggests that the wind velocity reversals reside on a fractal set of dimension D given by the magnitude of the power-law exponent. The dimension here is about 0.4 corresponding to the solid line. Larger scales are space-filling and follow the dashed line representing r^{-1}. The inset shows the variation of the fractal dimension with Ra.

for both, but its range is significantly greater for the higher Ra, extending mainly to much lower frequencies. This confirms the qualitative feature that there are only short-lived reversals of wind velocity at lower Ra. The cross-over frequency between the flat and power-law regions varies roughly as $Ra^{-2/3}$, at least below $Ra \approx 10^{11}$.

Since it is the dynamics of wind velocity reversals between two nominally constant values that concerns us mainly, it is useful to consider the set of points along the time axis corresponding to the zero crossings of $V(t)$, i.e. points corresponding to wind velocity reversals. Specifically, we divide this entire set into boxes of size r and count the number of non-empty boxes, N_r, that is boxes that contain at least one zero crossing. For a fractal we should have by standard definition

$$N_r \sim r^{-D}, \tag{3.2}$$

where D is the dimension of the set. A typical plot of log N_r vs. log r is given in figure 7 for one particular value of Ra. The shorter crossing scales (roughly below twice the mean crossing scale) possess a plausible power law with a negative slope of about 0.4, while the larger scales are clearly space-filling with $N_r \propto 1/r$. The fractal dimension evaluated in this way is plotted as the inset to figure 7 for various Ra. It appears that the dimension saturates near 0.4.

The switching process observed in this flow seems to have analogues in other instances as well: for example, paleomagnetic records show non-periodic and 'sudden' reversals in the polarity of the dipolar part of Earth's magnetic field. These polarity reversals have also been observed in the simulations of Earth's dynamo (see e.g. Glatzmaier *et al.* 1999). Various models of such phenomena are possible, but since the phenomenon in the present instance is thermal in origin, a brief discussion of the structure of temperature fluctuations is now in order.

4. Thermal plumes

The temperature trace of figure 3, a segment of which is expanded in the upper right inset to figure 8, displays a characteristic periodicity. This periodicity is confirmed by

a peak in the power spectral density as well as a small harmonic (figure 8). The peak has been detected in previous measurements, e.g. Castaing *et al.* (1989), Ciliberto *et al.* (1996), Qiu, Yao & Tong (2000). While it may not follow a pure power law (Villermaux 1995), the circular peak frequency (see lower left inset to figure 8) in the present experiments can be described, to a good approximation, by the scaling

$$\omega_p L^2/\kappa = 0.64 Ra^{0.47}, \tag{4.1}$$

which is in good agreement with the data of Castaing *et al.* (1989).†

The presence of the spectral peaks, signifying a modulation of the temperature signal, is thought to be associated with 'plumes' ejected from the thermal boundary layers. In the model proposed by Howard (1966), a layer of fluid subject to a uniform but high heat flux allows the growth of a diffusive boundary layer until it reaches a supercritical size, whereupon it may eject a plume. This describes, then, a periodic process with period T^*, based on these arguments, given by

$$T^* = (2Ra_{cr}\nu\kappa/g\alpha\Delta)^{2/3}/\kappa \tag{4.2}$$

or

$$\omega^* L^2/\kappa = 0.037 Ra^{2/3}, \tag{4.3}$$

using a plausible value for the critical Rayleigh number Ra_{cr} (say 1100, appropriate to convection in a box with one rigid and one free surface, see Chandrasekhar 1961).

Equation (4.3) yields a scaling that is in good agreement with various plume frequency measurements in the absence of any wind (e.g. Schaeffer & Manga 2001). It gives a frequency of magnitude similar to the present measurements at the lowest Ra but becomes an increasingly poorer approximation as Ra increases (compare (4.3) and (4.1)). Defining $\Lambda = \omega_p/\omega^*$ we find that Λ is near unity for $Ra \simeq 4 \times 10^6$ but decreases as $\Lambda \approx 18 Ra^{-1/5}$, where the exponent here is obviously just the difference between the two power-law exponents corresponding to (4.1) and (4.3). It is clear that some new physics, different from these plumes, is in operation.

Some sense of this physics can be obtained by noting the relation between the peak frequency (4.1) and the wind speed. The time taken by the wind to traverse the apparatus once is given by

$$4L/V_M \sim L^2/\kappa Ra^{1/2} \sim 1/\omega_p, \tag{4.4}$$

where we have used (3.1) and (4.1) in the two steps above, respectively, and ignored a small discrepancy in the power-law exponents (see the comment on exponents below (3.1)). Signals from two sensors mounted 180° about the azimuth from one another have the largest correlation when the time delay between them is set precisely by equation (4.4). Indeed, (4.4) is suggestive of a self-organization in turbulent convection between the production of plumes and the wind that carries them. In this respect,

† This frequency is substantially larger than that measured by Takeshita *et al.* (1996) and Cioni, Ciliberto & Sommeria (1997) for mercury, which shows that the Prandtl number of the fluid has a discernible influence on the magnitude of this frequency. These peaks are visible, though considerably weaker, even in the temperature traces measured near the centre of the apparatus for $\Gamma = 1$ but not for $\Gamma = 1/2$, this being a major difference between the two cases. The power spectra reveal in addition a weak but consistently present harmonic, to which little attention has been paid in the past; to explain this, Villermaux (1995) proposed a model in which the top and bottom boundary layers of the box couple to each other through the mean wind. It may be noted that, for frequencies higher than the peaks, the spectral slope is $-7/5$ for some range; higher frequencies for which buoyancy effects are negligible possess the classical $-5/3$ power, and even higher frequencies decay exponentially (see Niemela *et al.* 2000).

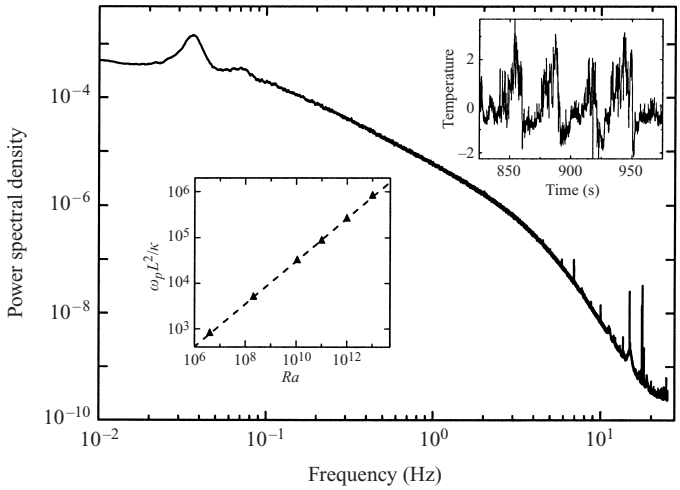

FIGURE 8. Power spectral density of the temperature signal from one of the sensors used to measure the wind velocity (expressed in arbitrary units); $Ra = 1.5 \times 10^{11}$. Periodic features are evident in the expanded view of the temperature trace shown in the upper right inset. This periodicity manifests itself as a strong peak in the power spectral density and a weak harmonic. The lower left inset shows the normalized peak frequency ω_p as a function of Ra.

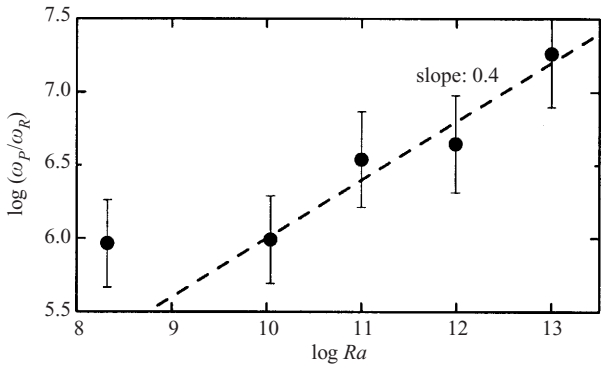

FIGURE 9. The ratio of plume frequency ω_P to the average reversal frequency ω_R. Beyond $Ra \approx 10^{10}$ the ratio increases like $Ra^{2/5}$ as shown by the dashed line. For $Ra > 10^{13}$, the measurement of the wind is uncertain (see text).

Villermaux (1995) describes a self-organizing scheme in which the top and bottom boundary layers act as two oscillators coupled by a large-scale re-circulating flow.

With increasing Ra, at least beyond 10^{10}, the plume frequency increases faster than the average reversal frequency ω_R. Their ratio is plotted in figure 9 and shows an increase at high Ra of the form $\omega_P/\omega_R \propto Ra^{2/5}$. In this sense, it is not clear that the notion of a 'steady' wind has much physical reality at very high Ra; it may more sensibly be thought of as increasingly frequent and disorganized large-scale lumps of hotter or colder fluid arriving at the measurement position. Indeed, beyond an Ra of 10^{13}, the excursions from V_M become more pronounced and it is difficult to specify the wind speed or direction with sufficient certainty. The situation is presumably complicated by the fact that the viscous boundary layer on the sidewall becomes increasingly thinner with increasing Ra, so that the fixed sensors are increasingly subject to the turbulent fluctuations characteristic of the central region.

5. Speculations on the reversal of the wind direction

The source of reversals of the wind direction is not clear. We note that, for example, for $Ra = 1.5 \times 10^{11}$ the mean interval between two successive reversals is about 2500 s (see figure 3), whereas that between the periodic features of the temperature signal is about 30 s (see figure 8). This orders-of-magnitude difference persists at all Rayleigh numbers.

The sudden reversals in the wind direction may come about as follows. Assume that the wind is created as described in § 4. When a plume is generated, it carries with it some heat and the fluid suffers a partial loss of buoyancy. If a 'hot' plume, say, is released close to where the buoyancy operates most effectively, namely near the sidewall, it is natural to think that the upward motion of the fluid along the sidewall will be retarded. A chance occurrence near the wall of a number of neighbouring plumes, or of one very large plume, might extract enough heat that the boundary layer cannot any longer traverse up the sidewall. At this point, a small perturbation could initiate the motion of the boundary layer up the same wall again, or up the opposite wall. Thus, a reversal may be a combination of both the large chance event and some small perturbation whose directional impact cannot be determined *a priori*.

6. Summary remarks

We have explored the dynamics of the wind in convection by considering velocity data from very long time series at various Rayleigh numbers between 10^6 and 10^{16}. We have obtained quantitative data on some of the statistical properties such as its reversal frequency, and expressed them as various power laws. It is conceivable that power-law expressions of this nature are merely convenient correlators of data, rather than representations of more fundamental physics. The main qualitative lesson is that the interaction between thermal plumes and the wind reversal is strong. A further basic conclusion may be that the reversal of wind direction is brought about by a chance occurrence of some large plume, or a collection of plumes, and a small perturbation.

The work has had the benefit of comments by numerous colleagues, among whom are: Roberto Benzi, Friedrich Busse, Bernard Castaing, Sergio Ciliberto, Charles Doering, Siegfried Grossmann, Robert Kerr, Detlef Lohse, Horst Meyer, Edward Ott, Itamar Procaccia, Seth Putterman, Paul Roberts, Patrick Tabeling and Emmanuel Villermaux. The research was supported by the NSF grant DMR-95-29609.

REFERENCES

Ashkenazi, S. & Steinberg, V. 1999 High Rayleigh number turbulent convection in a gas near the gas-liquid critical point. *Phys. Rev. Lett.* **83**, 3641–3644.

Castaing, B., Gunaratne, G., Heslot, F., Kadanoff, L., Libchaber, A., Thomae, S., Wu, X. Z., Zaleski, A. & Zanetti, G. 1989 Scaling of hard thermal turbulence in Rayleigh–Bénard convection. *J. Fluid Mech.* **204**, 1–30.

Chandrasekhar, S. 1981 *Hydrodynamic and Hydromagnetic Stability*. Dover, New York.

Ciliberto, S., Cioni, S. & Laroche, C. 1996 Large-scale properties of turbulent thermal convection. *Phys. Rev.* E **54**, R5901–R5904.

Cioni, S., Ciliberto, S. & Sommeria, J. 1997 Strongly turbulent Rayleigh–Bénard convection in mercury: comparison with results at moderate Prandtl number. *J. Fluid Mech.* **335**, 111–140.

Glatzmaier, G. A., Coe, R. C., Hongre, L. & Roberts, P. H. 1999 The role of the Earth's mantle in controlling the frequency of geomagnetic reversals. *Nature* **401**, 885–890.

Howard, L. N. 1966 Convection at high Rayleigh number. *Proc. 11th Intl Congr. on Applied Mechanics* (ed. H. Görtler), pp. 1109–1115. Springer.

Kadanoff, L. P. 2000 Turbulent heat flow: Structures and scaling. *Phys. Today* **54**, 34–39.

Kerr, R. M. 1996 Heat transport in convection and the asymptotic state. *J. Fluid Mech.* **310**, 139–179.

Krishnamurti, R. & Howard, L. N. 1981 Large scale flow generation in turbulent convection. *Proc. Natl Acad. Sci. USA* **78**, 1981–1985.

Niemela, J. J., Skrbek, L., Sreenivasan, K. R. & Donnelly, R. J. 2000 Turbulent convection at very high Rayleigh numbers. *Nature* **404**, 837–840.

Qui, X.-L., Yao, S.-H. & Tong, P 2000 Large-scale coherent rotation and oscillation in turbulent thermal convection. *Phys. Rev.* E **61**, R6075–R6079.

Sano, M., Wu, X. Z. & Libchaber, A. 1989 Turbulence in helium gas free convection. *Phys. Rev.* A **40**, 6421–6430.

Schaeffer, N. & Manga, M. 2001 Interaction of rising and sinking mantle plumes. *Geophys. Res. Lett.* **28**, 455–458.

Takeshita, T., Segawa, T., Glazier, J. A. & Sano, M. 1996 Thermal turbulence in mercury. *Phys. Rev. Lett.* **76**, 1465–1468.

Villermaux, E. 1995 Memory-induced low frequency oscillations in closed convection boxes. *Phys. Rev. Lett.* **75**, 4618–4621.